ACS APPLIED MATERIALS & INTERFACES

Research Article

www.acsami.org

Modulation of Amyloid-β Fibrils into Mature Microrod-Shaped Structure by Histidine Functionalized Water-Soluble Perylene Diimide

Balakrishnan Muthuraj,[†] Sayan Roy Chowdhury,[†] and Parameswar K. Iyer*[,†,‡]

[†]Department of Chemistry, Indian Institute of Technology, Guwahati 781039, Assam, India

[‡]Center for Nanotechnology, Indian Institute of Technology, Guwahati 781039, Assam, India

Supporting Information

ABSTRACT: Alzheimer's disease (AD) is associated with different types of amyloid peptide aggregates including senile plaques, fibrils, protofibrils, and oligomers. Due to these difficulties, a powerful strategy is needed for the disaggregation of amyloid aggregates by modulating their self-aggregation behavior. Herein, we report a unique approach toward transforming the aggregated amyloidogenic peptides using an amino acid functionalized perylene diimide as a molecular modulator, which is a different nondestructive approach as compared to inhibiting the aggregation of peptides. The histidine functionalized perylenediimide (PDI−HIS) molecule could coassemble with amyloid β (Aβ) peptides via hydrogen bonding that leads to the enhancement in the $\pi-\pi$ interactions between Aβ and PDI−HIS moieties. The Thioflavin T (ThT) assay and various spectroscopic and microscopic techniques establish that the PDI−HIS molecules accelerate the Aβ1−40 and the amyloid aggregates in CSF into micro size coassembled structures. These results give rise to a new and unique complementary approach for modulating the biological effects of the aggregates in amyloidogenic peptides.

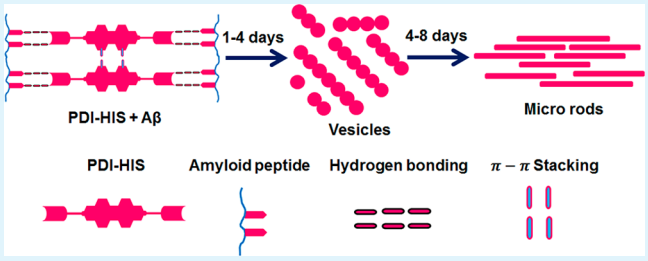

KEYWORDS: *amyloid-β peptides, aggregation, molecular modulator, perylene diimide, neurodegenerative disease, self-assembly*

INTRODUCTION

The aggregation of soluble Aβ monomer or oligomers into insoluble plaques or amyloid fibrils is a crucial step that drives Alzheimer's disease (AD) pathogenesis.[1−4] Based on this hypothesis several effective protocols have been attempted to modulate or inhibit Aβ, such as peptides,[5,6] antibodies,[7,8] metal ion chelators,[9,10] small molecules,[11,12] and nanoparticles,[13−16] which gave certain beneficial results toward AD treatment by preventing Aβ aggregate progression. Thus, an attractive therapeutic strategy for AD treatment remains the effective preservation mechanism of Aβ homeostasis by a combination of inhibiting Aβ aggregation and promoting Aβ aggregate clearance.

Small molecule based probes can self-assemble into well-arranged superstructures with multiple noncovalent interactions like hydrogen-bonding (H-bonding) and $\pi-\pi$ interactions.[17,18] Notably, the noncovalent interactions are the driving forces for the peptide−organic molecule interaction and could lead to the efficient coassembly process.[18−22] Hence, the efficient coassembly between peptide and organic molecules is a vital structural characteristic of peptide assembly study for peptide-induced diseases such as AD, Parkinson's disease, and prion diseases. Currently, smart self-assembling molecules have been identified that associate and promote the peptide−peptide and peptide−organic interactions converting the Aβ monomers and oligomers into nontoxic forms since the oligomeric forms of amyloidogenic peptides are reported to have higher toxicity as compared to the fibrillar aggregates.[11,12,23−29] In the present study, we establish a complementary approach to achieve a hybrid structure in the form of microrods from aggregated Aβ fibrils by the coassembly between Aβ1−40 fibrils and histidine functionalized perylenediimide (PDI−HIS) molecule (Scheme 1).[30−32]

EXPERIMENTAL SECTION

Materials. All the reagents and chemicals were purchased from Aldrich Chemicals, Merck or Ranbaxy (India) and were used as received. Milli-Q water and HPLC grade solvents were used in all the experiments. Solvents were degassed using three freeze thaw cycles or flushed with nitrogen for at least 1 h prior to use when necessary. β-Amyloid (1−40), human was purchased from GL Biochem, Ltd., Shanghai, China. The cerebrospinal fluid (CSF) samples were gifted by Guwahati Neurological Research Center and Hospital, Guwahati, India, and were obtained as part of routine care from patients. Nonetheless, information explaining the purpose of this study was specified at the time of sample collection, adhering to the bioethics policy of the hospital.

Instrumentation. Fluorescence spectra were carried out on a FluoroMax-4 Spectrofluorometer-Horiba Scientific. A 10 × 10 mm quartz cuvette was used for solution spectra and emission was collected at 90° relative to the excitation beam. Leica polarizable optical microscope was used to image the aggregation and disruption studies.

Received: June 12, 2015
Accepted: September 4, 2015
Published: September 4, 2015

DOI: 10.1021/acsami.5b07260
ACS Appl. Mater. Interfaces 2015, 7, 21226−21234

Scheme 1. Schematic Representation of Microrod Formations from Aggregated Aβ1−40 with PDI−HIS

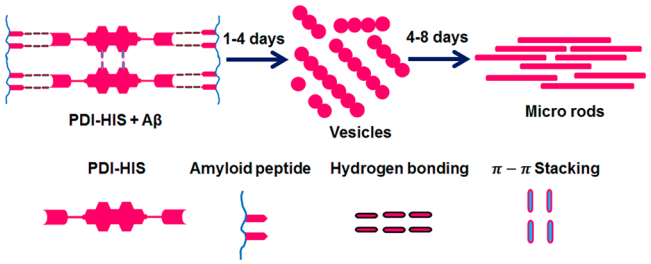

FT−IR spectra were recorded on a PerkinElmer spectrometer with samples prepared as KBr pellets. A fresh glass slide was used for every experiment. Deionized water was obtained from Milli−Q system (Millipore). Field emission scanning electron microscopy (FE-SEM) measurements were made on a Carl Zeiss, SIGMA VP instrument. Atomic force microscopy (AFM) was recorded on Agilent, Model 5500 series with noncontact mode. DLS were measured by Zetasizer Nano series Nano-ZS90 instrument. The POM images were obtained on a Leica DM 2500P microscope.

Synthesis of PDI−HIS. First, 3,4,9,10-perylenetetracarboxylic acid bisanhydride (500 mg, 1.27 mmol), histidine (800 mg, 3.82 mmol) and 2.0 g of imidazole were heated at 140 °C for 8 h with stirring. The reaction mixture was allowed to cool to 90 °C and then poured into water. Then, the mixture was acidified with 2.0 M HCl and the precipitate was washed with water and dried under vacuum at 80 °C to give the product of PDI−HIS (800 mg, 94%).[33]

Cell Viability Assay (MTT). Viability of HUVEC, EA.hy926, A549, and B16 cells were checked by MTT assay as per published protocol.[33] Initially, 10 000 cells/well were seeded in per well of 96 well plate and different concentrations of probe PDI−HIS (10−750 μg/mL) was added for cytotoxicity experiment for 24 h as a dose-dependent manner. After 48 h treatment, 1 mL MTT stock solution (concentration 5 mg/mL) was diluted to 10 mL solution using DMEM media and 100 μL of this MTT solution (10 μL 5 mg/mL MTT + 90 μL of corresponding media) was added to each well by replacing the media and further allowed to incubate for 4 h. After 4 h, the media in each well was replaced by 100 μL of DMSO−methanol mixture (1:1 v/v) for solubilizing the violet crystal and kept the mixture on the shaker for homogeneous mixture. Finally, the absorbance of the mixture was measured at 570 nm using a microplate reader (Varioskan Flash). All the experiments were carried out in triplicate, and the results are expressed as normalized viability = $\{1/\mathrm{Abs}_{\lambda} = 570\ (\text{untreated cells} - \text{blank})\} \times \{\mathrm{Abs}_{\lambda} = 570\ (\text{treated cells} - \text{blank})\}$.

Preparation of Stock Solutions. The PDI−HIS stock solution was prepared at a concentration of 1.0×10^{-3} mL^{-1} in 10 mL H_2O at pH 7−9. This stock solution was diluted to desired concentration for each titration in a 3 mL cuvette with 10 mM HEPES buffer at pH 7.4.

Preparation of HEPES Buffer Solutions. The fluorescence titrations and all other experiments were performed in 10 mM HEPES buffer solution, and pH 7.4 was maintained by using 4 M NaOH or 5 M HCl solution.

TFA/HFIP Treatment of Aβ1−40. Aβ1−40 was disaggregated using trifluoroacetic acid/1,1,1,3,3,3-hexafluuor-2-propanol (TFA/HFIP) by an established method.[34−36] First, 0.5 mg of Aβ1−40 was added to a 2.5 mL Eppendorf tube and dissolved in TFA to obtain a homogeneous solution free of aggregates. TFA was then evaporated using argon gas. Any left-over TFA was further removed by adding HFIP followed by evaporation using an argon gas flow to obtain a film like material. This process was repeated twice. To the Eppendorf tube was added 2.5 mL of HEPES (10 mM, pH 7.4) followed by sonication and vortexing to obtain a final concentration of 4.6×10^{-4} M. Fibril formation was monitored using a ThT binding assay.

Preparation of Aβ1−40 Aggregates and ThT Binding Assay. For the preparation of amyloid peptide aggregates,[34−37] after the TFA/HFIP treatment for amyloid peptide, the Aβ1−40 (25 μM) was initially incubated with ThT (20 μM) at 37 °C for 0−72 h in 10 mM HEPES buffer at pH 7.4 with steady agitation. Further, Aβ1−40 aggregated amyloid fibrils were monitored with different time incubations by monitoring ThT (20 μM) fluorescence enhancement peak at $\lambda_{em} - 488$ nm while exciting at $\lambda_{ex} - 440$ nm.

Confirmation of CSF Aβ Aggregates using ThT Binding Assay. The presence of Aβ fibrils in CSF was confirmed by the gradual addition of CSF sample up to 100 μL solution (each addition, 10 μL) into ThT (20 μM) solution (pH 7.4 in HEPES) to observe a gradual enhancement in the fluorescence intensity of ThT at 488 nm validating strongly the existence of aggregated Aβ fibrils in the CSF sample (Figure S2).

Modulating Experiment for Aβ1−40 and CSF Aggregates. The modulating ability of PDI−HIS was examined by the changes in the fluorescence spectra in the presence of Aβ1−40 fibrils and CSF Aβ fibrils. The samples were prepared in the final volume of 3000 μL in HEPES buffer (10 mM, pH 7.4). First, when PDI−HIS (0.33 μM) solution was excited at 508 nm, we observed an emission peak at 546 nm. Further, upon addition of Aβ1−40 fibrils (0.76 μM) and CSF Aβ fibrils (50 μL) into the PDI−HIS solution, the fluorescence changes observed instantly in PDI−HIS + Aβ1−40 and PDI−HIS + CSF aggregate mixtures were minimum. However, after incubation (0−90 h) at 37 °C (pH 7.4), we observed gradual fluorescence enhancement in the PDI−HIS + Aβ1−40 and PDI−HIS + CSF solutions, respectively.

AFM Sample Preparation. As-prepared solutions of PDI−HIS (0.33 μM) + Aβ1−40 (0.76 μM) and PDI−HIS (0.33 μM) + CSF (50 μL) aggregates were kept in 3 mL of HEPES buffer (10 mM, pH 7.4) for 0−90 h incubation at 37 °C in water bath. These solutions were further utilized to monitor the AFM morphology. Both the solutions were separately diluted by 10 times and then from the diluted solutions 5 μL of the PDI−HIS + Aβ1−40 and PDI−HIS + CSF samples were drop-casted onto freshly cleaned glass slide and dried at room temperature overnight and recorded by atomic force microscopy (AFM) on Agilent, Model 5500 series with noncontact mode.

FE-SEM Sample Preparation. As-prepared solutions of PDI−HIS (0.33 μM) + Aβ1−40 (0.76 μM) and PDI−HIS (0.33 μM) + CSF (50 μL) aggregates were kept in 3 mL of HEPES buffer (10 mM, pH 7.4) for 0−90 h incubation at 37 °C in water bath. These solutions were further utilized to monitor the FE-SEM morphology. Both solutions were separately diluted by 10 times, and then, from the diluted solutions, 5 μL of the PDI−HIS + Aβ1−40 and PDI−HIS + CSF samples were drop-casted onto the aluminum foil covered freshly cleaned glass slide and dried at room temperature overnight and recorded by field emission scanning electron microscopy (FE-SEM) on a Carl Zeiss, SIGMA VP instrument.

FT-IR spectra sample preparation. As-prepared solutions of PDI−HIS (0.33 μM) + Aβ1−40 (0.76 μM) and PDI−HIS (0.33 μM) + CSF (50 μL) aggregates were kept in 3 mL of HEPES buffer (10 mM, pH 7.4) for 0−90 h incubation at 37 °C in water bath. These solutions were further utilized to monitor the FT-IR spectra. 30−50 μL of PDI−HIS + Aβ1−40 fibrils and PDI−HIS + CSF samples were drop-casted onto the freshly cleaned glass slide and dried at room temperature overnight and FT−IR spectra recorded on a PerkinElmer spectrometer with samples prepared as KBr pellets.

Dynamic Light Scattering Study. As-prepared solutions of PDI−HIS (0.33 μM) + Aβ1−40 (0.76 μM) and PDI−HIS (0.33 μM) + CSF (50 μL) aggregates were kept in 3 mL of HEPES buffer (10 mM, pH 7.4) for 90 h incubation at 37 °C in water bath. These solutions were further utilized to monitor the hydrodynamic particle diameter by DLS. Both the solutions were separately diluted by 10 times, and then, from the diluted solution, 500 μL of the PDI−HIS + Aβ1−40 and PDI−HIS + CSF samples were used to record DLS measurements by Zetasizer Nano series Nano-ZS90 instrument.

Polarized Optical Microscopy Study. Images of Aβ1−40 and CSF aggregates were detected by optical microscopy. Aβ1−40 aggregates (0.76 μM) were incubated with PDI−HIS (0.33 μM) in 3 mL of HEPES buffer solution (10 mM, pH 7.4) at 37 °C for 0−90 h. Similarly, CSF aggregates (50 μL) were also incubated with PDI−HIS (0.33 μM) in 3 mL of HEPES buffer solution (10 mM, pH 7.4) at 37 °C for 0−90 h. Further, from the above solutions the samples were prepared separately by spreading 30 μL of each solution on glass slide and the images were observed for both the samples at different time of

DOI: 10.1021/acsami.5b07260
ACS Appl. Mater. Interfaces 2015, 7, 21226−21234

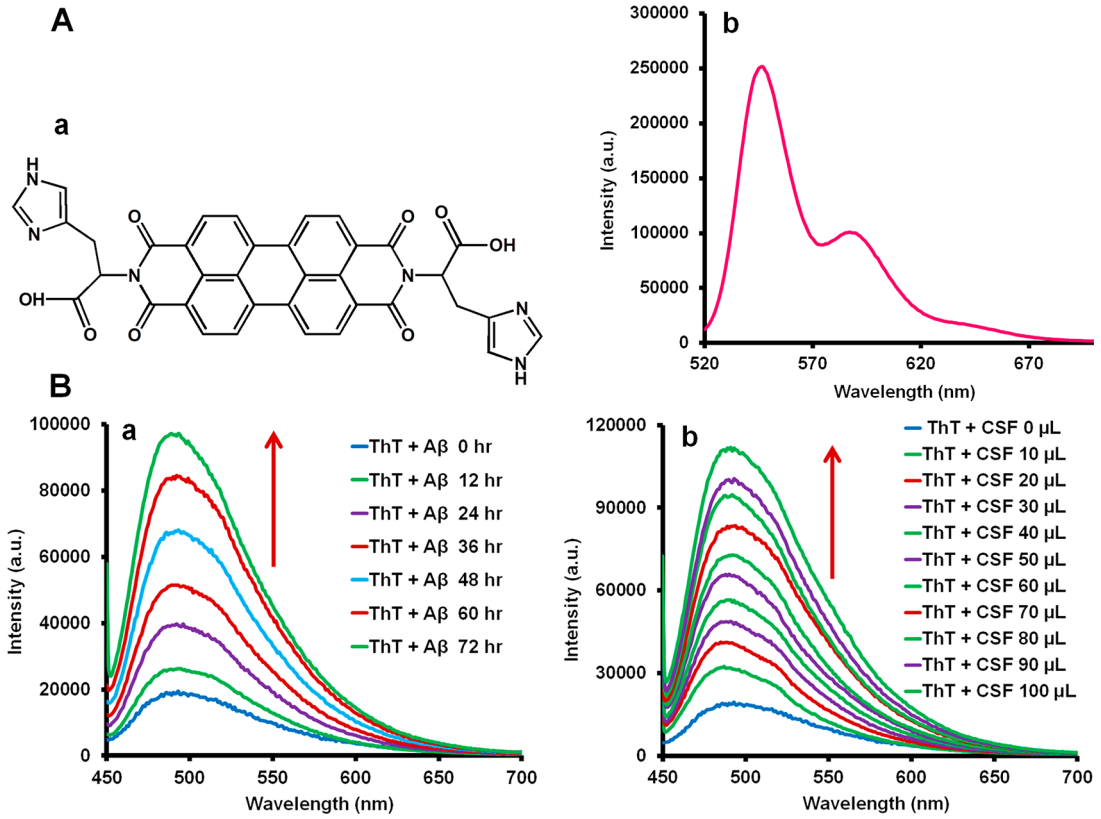

Figure 1. (A, a) The structure of PDI−HIS and (A, b) fluorescence spectra of PDI−HIS (0.33 μM) in HEPES buffer solution at pH 7.4. (B) Detection of Aβ fibrils using ThT assay; (B, a) fluorescence enhancement spectra (λ_{ex} = 440 nm, λ_{em} = 488 nm) of ThT (20 μM) (pH 7.4 in HEPES) mixed Aβ1−40 (25 μM) was measured every interval incubation time from 0 to 72 h, and (B, b) fluorescence enhancement (λ_{ex} = 440 nm, λ_{em} = 488 nm) of ThT (20 μM) (pH 7.4 in HEPES) was observed on addition of CSF (0−100 μL).

incubation under Leica DM 2500P microscope. For control study, we performed similar experiments to confirm the formation of coassembled vesicles and mature rod-shaped structures in the absence of PDI−HIS with Aβ 1−40 fibrils (0.76 μM) and CSF Aβ fibrils (50 μL) after 4 and 8 days incubation. The obtained images show that the mature rod-shape structures were not observed in the absence of PDI−HIS with Aβ 1−40 fibrils as well as with CSF Aβ fibrils, even after 4 and 8 days incubation.

RESULTS AND DISCUSSION

Herein, we report a histidine functionalized biocompatible (See Supporting Information) molecule PDI−HIS (λ_{em} = 546 nm) which is used as a modulator for Aβ aggregates (Figure 1A).[33] The formation of coassembly with Aβ1−40 fibrils and Aβ aggregates in real cerebrospinal fluid (CSF) which is a vital biomarker for AD is presented using thise water-soluble PDI−HIS molecule. The modulating effects of PDI−HIS on Aβ aggregates were validated using AFM, FE-SEM, DLS, Polarized optical microscopy (POM), optical spectroscopy, and Fourier transform infrared spectroscopy (FT-IR).

Confirmation for the Presence of Aβ Peptide Aggregates by ThT Assay. Thioflavin T (ThT) assay is one of the most widely used methods to identify Aβ fibrils with high sensitivity.[38,39] The emission band at 488 nm is expected to be directly proportional to the amount of Aβ fibrils present, consequently, the formation of Aβ fibrils can be easily followed by measuring ThT fluorescence enhancement by time-dependent manner. Upon addition of Aβ1−40 (25 μM) monomer into ThT (20 μM), a gradual enhancement of the emission peak at 488 nm is observed over 0−72 h incubation time (λ_{ex} − 440 nm) (Figure 1B, a) which indicates the presence of Aβ fibrils. ThT enhanced fluorescence occurs due to the changes in the rotational freedom of the C−C bonds between the benzothiazole and dimethylanilino rings.[40] Further, the presence of Aβ fibrils in CSF was also confirmed by the addition of up to 100 μL of the CSF sample into 20 μM solution of ThT (pH 7.4 in HEPES). After the addition of CSF sample a gradual enhancement in the fluorescence intensity of ThT at 488 nm was observed which validates strongly the existence of aggregated Aβ fibrils in the CSF sample (Figure 1B, b).[36,41] Because the Aβ fibrils formation from Aβ1−40 monomers and the existence of aggregated Aβ fibrils in the CSF sample is confirmed, we have further utilized these two samples for our studies.

Confirmation of the Presence of Aβ Peptide Aggregates by Microscopic Techniques. Several microscopy methods such as electron microscopy (EM) and atomic force microscopy (AFM) have been established to characterize the structural and morphological changes of noncrystalline protein fibrils.[42−44] The Aβ1−40 aggregates were monitored by AFM at different incubation times (Figure 2). The sample deposited with the freshly prepared solution showed both small and large oligomers as observed in the topography image (Figure 2a). The diameter of Aβ oligomers was observed to be ∼100 ± 10 nm and ∼5 nm height (Figure 2b,c). After the Aβ monomers and oligomers were incubated for 3 days, AFM showed a number of fibrils in the topography image (Figure 2d) with ∼80 ± 20 nm diameter and ∼4−6 nm height (Figure 2e,f) confirming that the monomers and dimers continue to form aggregated oligomers that further assemble to form protofibrils and then into fibrils. The images of the real CSF sample (Figure 2g−i) showed large number of mature fibrils. The diameter of Aβ fibrils in CSF was observed to

DOI: 10.1021/acsami.5b07260
ACS Appl. Mater. Interfaces 2015, 7, 21226−21234

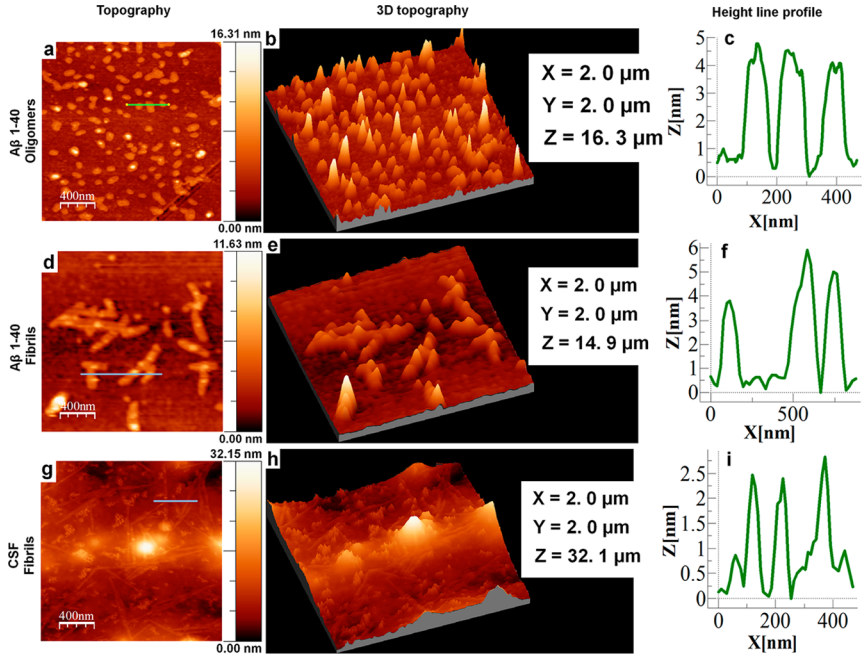

Figure 2. Detection of Aβ fibrils using AFM analysis. (a) Aβ oligomers, (d) Aβ fibrils (from Aβ 1−40) samples were analyzed after incubation times of (a) 24 and (d) 72 h. (g) Detection of Aβ Fibrils (from CSF). (b, e, and h) 3D Topography images of Aβ oligomers, Aβ fibrils, and CSF fibrils. (c, f, and i) Height line profiles of Aβ oligomers, Aβ fibrils, and CSF fibrils. (X = distance; Y = Height).

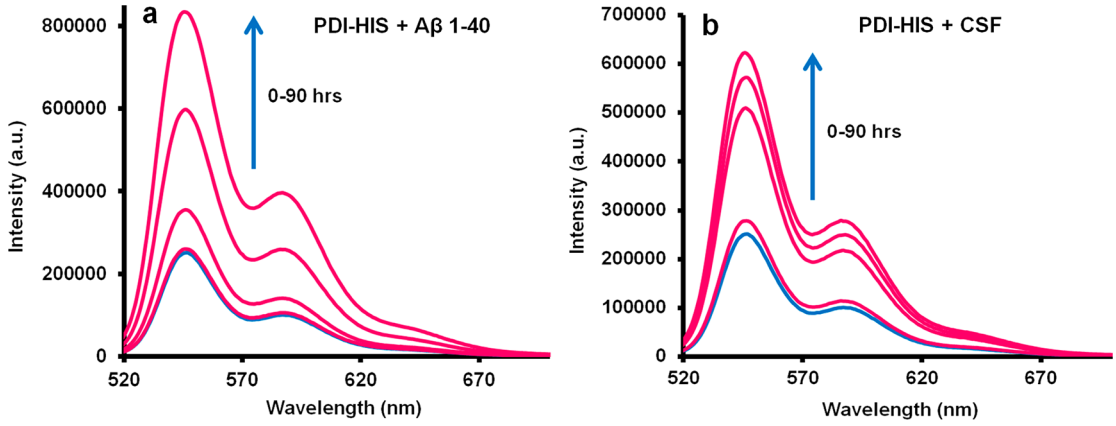

Figure 3. Fluorescence enhanced emission spectra measured for (a) PDI−HIS (0.33 μM) with Aβ1−40 (0.76 μM) aggregates and (b) PDI−HIS (0.33 μM) with CSF (50 μL) aggregates from 0 to 90 h incubation in HEPES (10 mM) buffer at pH 7.4. Excitation of PDI−HIS is 508 nm and emission at 546 nm maximum.

be ~50 ± 20 nm and ~2.5 nm height (Figure 2h,i). Consequently, these morphological results confirm that the formation of aggregated Aβ fibrils from Aβ1−40 monomers and the existence of Aβ fibrils in CSF could be used for further characterization.

Modulating Effect of PDI−HIS on Aβ Aggregates Monitored by Fluorescence Spectroscopy. Further, the binding and modulating ability of PDI−HIS were ascertained by the changes in the fluorescence spectra in the presence of Aβ1−40 fibrils and CSF Aβ fibrils. When PDI−HIS (0.33 μM) solution was excited at 508 nm we observed an emission peak at 546 nm (Figure 3 (a, b) blue curve). Upon separate addition of Aβ1−40 fibrils (0.76 μM) and CSF Aβ fibrils (50 μL) into the PDI−HIS solution, only slight fluorescence changes were observed in the PDI−HIS + Aβ1−40 fibrils and PDI−HIS + CSF aggregate mixtures. However, after the samples incubated for 0−90 h at 37 °C (pH 7.4), we observed gradual fluorescence enhancement in the PDI−HIS + Aβ1−40 fibrils and PDI−HIS + CSF solutions, respectively. The fluorescence enhancement occurred due to the formation of well-ordered supramolecular coassembly structures of Aβ1−40 and CSF aggregates with PDI−HIS via noncovalent interactions like H-bonding and $\pi-\pi$ stacking. The coassembly between PDI−HIS and Aβ aggregates likely occurs via the H-bonding between the hydrophilic ends of PDI−HIS with the Aβ peptide containing amide and carboxylic groups which further induces the formation of $\pi-\pi$ stacking between perylene hydrophobic interfaces. These noncovalent interactions promote the interconversion of the fibrillar structures into microrod-like structures (Scheme 1) as visualized and confirmed via other techniques (AFM, FE-SEM and POM images).

Modulating effect on Aβ Peptide Aggregates Monitored by FT-IR Spectra and DLS Study. To validate the results obtained from fluorescence study, we examined the secondary structure of Aβ1−40 fibrils alone and the coassembly

DOI: 10.1021/acsami.5b07260
ACS Appl. Mater. Interfaces 2015, 7, 21226−21234

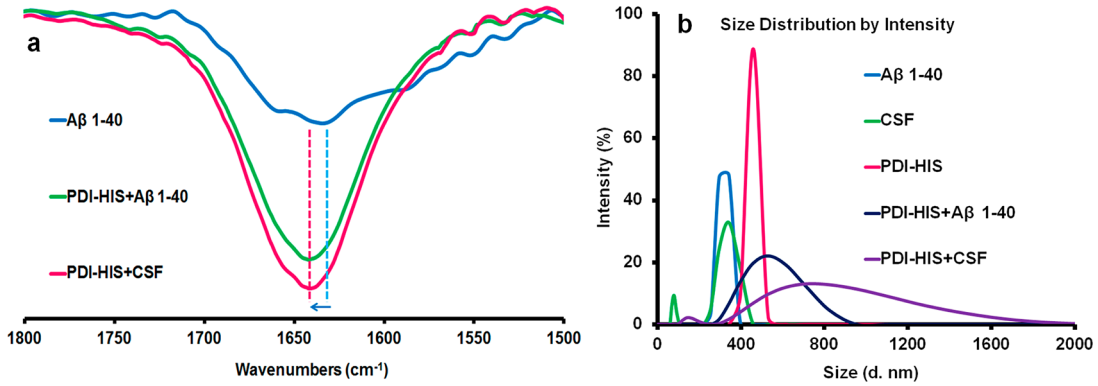

Figure 4. (a) Modulation effects of PDI−HIS on Aβ1−40 fibrils and CSF Aβ fibrils were measured by FT-IR spectroscopy. (b) Modulation effects of PDI−HIS on Aβ1−40 fibrils and CSF Aβ fibrils were measured by Dynamic light scattering (DLS) in HEPES buffer solution at pH 7.4.

structures of PDI−HIS + Aβ1−40 fibrils and PDI−HIS + CSF aggregates by using FT-IR spectroscopy.[45−47] The FT-IR spectrum of Aβ1−40 fibrils and CSF Aβ fibrils shows a major band at 1630 ± 2 cm^{-1} which indicates the parallel β-sheet conformation of Aβ1−40 aggregates (Figure 4a, blue curve, and Figure S3). The parallel β-sheet conformation of Aβ1−40 fibrils were transformed into the random coil conformation due to the formation of coassembly structures with PDI−HIS (PDI−HIS + Aβ1−40 fibrils and PDI−HIS+CSF Aβ fibrils), as illustrated by a major band at 1646 ± 2 cm^{-1} (Figure 4a, green and pink). This result confirms that PDI−HIS has the ability to modulate preformed Aβ1−40 fibrils as well as the Aβ aggregates in CSF.

Further, we examined the size distribution of PDI−HIS and the formation of coassembly structure between PDI−HIS and Aβ aggregates (Aβ1−40, CSF) in aqueous HEPES buffer (pH 7.4) solution by DLS experiments (Figure 4b). It could be established that the PDI−HIS could accelerate the formation of coassembly structure via aggregation process with Aβ1−40 fibrils as well as CSF Aβ fibrils (Figure 4b). The control experiments demonstrated that Aβ1−40 fibrils (295−341 d. nm), CSF Aβ fibrils (295−396 d. nm) and PDI−HIS (458 d. nm) are lower in size independently as compared to the coassembly structures of PDI−HIS+Aβ1−40 fibrils (342−825 d. nm) and PDI−HIS+CSF Aβ fibrils (342−1718 d. nm). Therefore, the mechanism of the accelerated aggregation during modulation could be attributed to the formation of coassembly by noncovalent interactions linking peptide stripes with the PDI−HIS molecules (Scheme 1). Therefore, it is feasible to change the Aβ aggregates (Aβ1−40, CSF) into coassembly structure in the presence of PDI−HIS. This result also strongly confirms that PDI−HIS modulates the aggregation behavior of Aβ1−40 fibrils and CSF Aβ fibrils, which would possibly reduce the effective concentration of Aβ self-aggregates.

Modulating effect on Aβ peptide aggregates monitored by morphology images. Furthermore, AFM and FE-SEM studies were also used to visualize the morphological images of the coassembly structure formation (Figure 5). As expected, Aβ1−40 monomers form Aβ1−40 fibrils and the existence of Aβ1−40 fibril in CSF were also confirmed by AFM and FE-SEM images as mentioned in earlier Figure 2d,g. In 3 mL of HEPES buffer (10 mM, pH 7.4) the prepared solutions of PDI−HIS (0.33 μM) + Aβ1−40 (0.76 μM) and PDI−HIS (0.33 μM) + CSF (50 μL) aggregates were kept for 0−90 h incubation at 37 °C in water bath. These solutions were further utilized to monitor the AFM morphology images. Both the solutions were separately diluted by 10 times and then from the diluted solutions, 5 μL of the PDI−HIS + Aβ1−40 and the PDI−HIS + CSF samples were drop-casted onto the freshly cleaned glass slide and dried at room temperature overnight, and the morphology was studied by AFM. Appreciably, microrod type morphology image developed when the PDI−HIS probe assembled with Aβ1−40 and CSF fibrils, rather than the formation of oligomer or fibrils (Figure 5A,B), which is an exceptional observation. The discrepancies in aggregate morphologies of Aβ1−40 and Aβ1−40 + PDI−HIS are very unique, which are assigned to the modulating effect on the assembly structures of Aβ1−40 peptides on a molecular level. The diameter of coassembled Aβ1−40 + PDI−HIS microrods were observed to be 550 ± 20 nm with ∼25 nm height and 6 ± 1 μm length (Figure 5A, a−c)), which are much bigger in size as compared to the free Aβ fibrils of amyloidogenic peptides. Similarly, the coassembled morphologies of CSF + PDI−HIS mature microrod diameter was observed to be 500 ± 10 nm with a height of ∼13 nm and length of 4 ± 1 μm (Figure 5A, d−f)). Additionally, FE-SEM also strongly supported the formation of coassembled mature microrod structures in the presence of PDI−HIS with Aβ1−40 and CSF aggregates respectively (Figure 5B). These results validate that PDI−HIS is an effective modulator for Aβ1−40 fibrils and Aβ aggregates in CSF by the interconversion of Aβ aggregates into coassembled mature microrod like structures that are completely different from the free Aβ fibrils.

The modulating effect of PDI−HIS on the assembly of Aβ1−40 and aggregated fibrils in CSF were also investigated by polarized optical microscopy (POM) (Figure 6). The POM images of Aβ1−40 and CSF aggregates depicted typical spherical shape (Figure 6a,e). Aβ1−40 aggregates (0.76 μM) were incubated with PDI−HIS (0.33 μM) in 3 mL of HEPES buffer solution (10 mM, pH 7.4) at 37 °C for 0−90 h. Similarly, CSF aggregates (50 μL) were also incubated with PDI−HIS (0.33 μM) in 3 mL of HEPES buffer solution (10 mM, pH 7.4) at 37 °C for 0−90 h. Further, from the above solutions the samples were prepared separately by spreading 30 μL of each solution on glass slide and the images were observed for both the samples at different time of incubation under a microscope. After 2 days incubation with PDI−HIS, the mixture of PDI−HIS + Aβ 1−40 aggregates and PDI−HIS + CSF aggregates showed the formation of coassembled vesicles (Figure 6b,f) due to the noncovalent interactions between the hydrophilic ends of the PDI−HIS with Aβ peptide containing amide and carboxylic groups as discussed earlier. This noncovalent interaction

DOI: 10.1021/acsami.5b07260
ACS Appl. Mater. Interfaces 2015, 7, 21226−21234

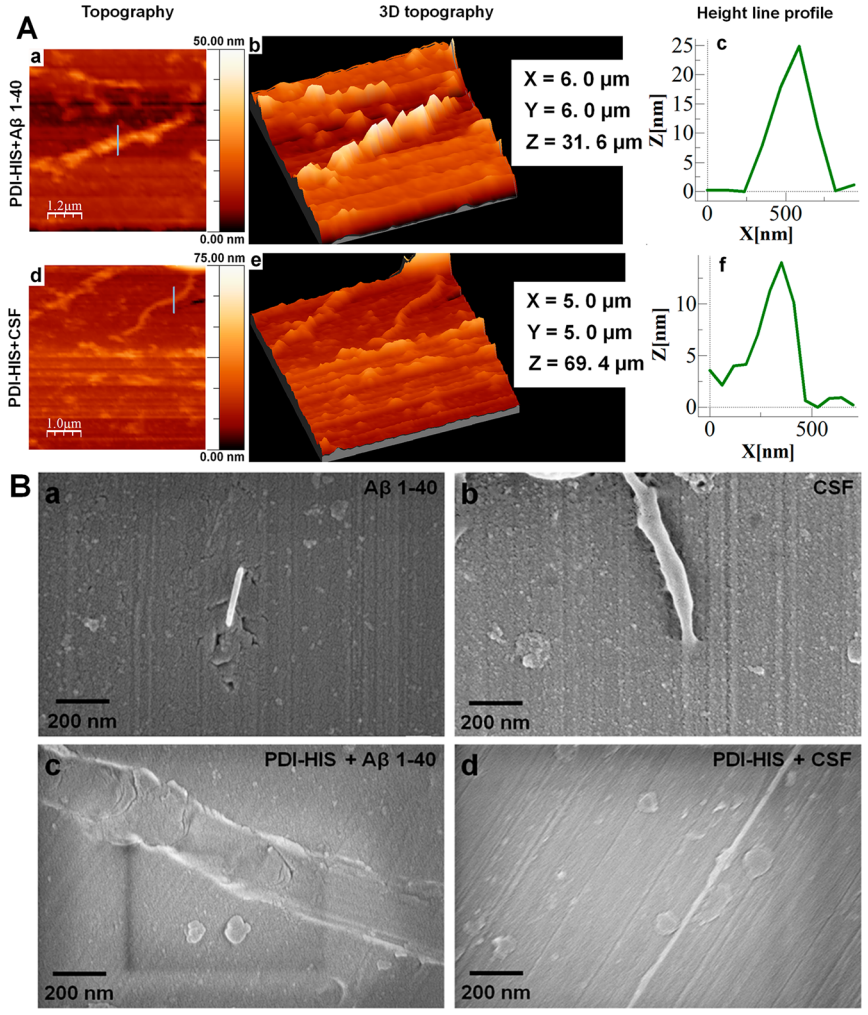

Figure 5. (A) Detection of Aβ1−40 fibrils during the formation of coassembled mature rod-shaped structure using PDI−HIS. (a) PDI−HIS + Aβ 1−40 fibrils (d) PDI−HIS with CSF Aβ fibrils after 8 days incubation. (b and e) 3D Topography images of PDI−HIS + Aβ1−40 fibrils and PDI−HIS + CSF Aβ fibrils. (c and f) Height line profiles of PDI−HIS + Aβ1−40 fibrils and PDI−HIS + CSF Aβ fibrils. (X = distance; Y= Height). (B) FE-SEM images demonstrate the modulating effect on Aβ1−40 and CSF aggregates into mature rod-shaped coassembly structure. (a and b) Aβ1−40 and CSF aggregates. (c and d) Coassembly structures of PDI−HIS + Aβ1−40 fibrils and PDI−HIS + CSF Aβ fibrils.

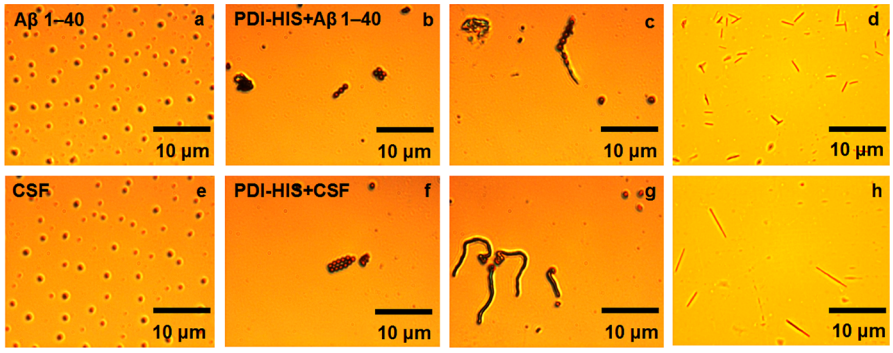

Figure 6. Detection of Aβ 1−40 fibrils into rod shaped coassembly structure using PDI−HIS. (a) Optical microscopic image clearly shows the formation of aggregated Aβ1−40 spheres. (b and c) The formation of coassembled vesicles and immature rod-shaped structures were observed in the presence of PDI−HIS (0.33 μM) with Aβ1−40 (0.76 μM) after 2 and 4 days incubation. (d) Formation of coassembled mature rod-shape structure was observed from vesicles structure by PDI−HIS with Aβ1−40 fibrils after 8 days incubation. (e) Optical microscopic image clearly shows the existence of aggregated Aβ spheres in CSF; (f, g) Formation of coassembled vesicles and immature rod-shape structures were observed in the presence of PDI−HIS (0.33 μM) with CSF Aβ fibrils (50 μL) after 2 and 4 days incubation. (h) Formation of coassembled mature rod-shape structure was observed from vesicles by PDI−HIS with CSF after 8 days incubation.

comprising $\pi-\pi$ stacking of PDI induces the formation of young microrod like structure after 4 days incubation at pH 7.4 in HEPES buffer solution (Figure 6c,g). However, when the same sample was incubated for 8 days the young and immature

DOI: 10.1021/acsami.5b07260
ACS Appl. Mater. Interfaces 2015, 7, 21226−21234

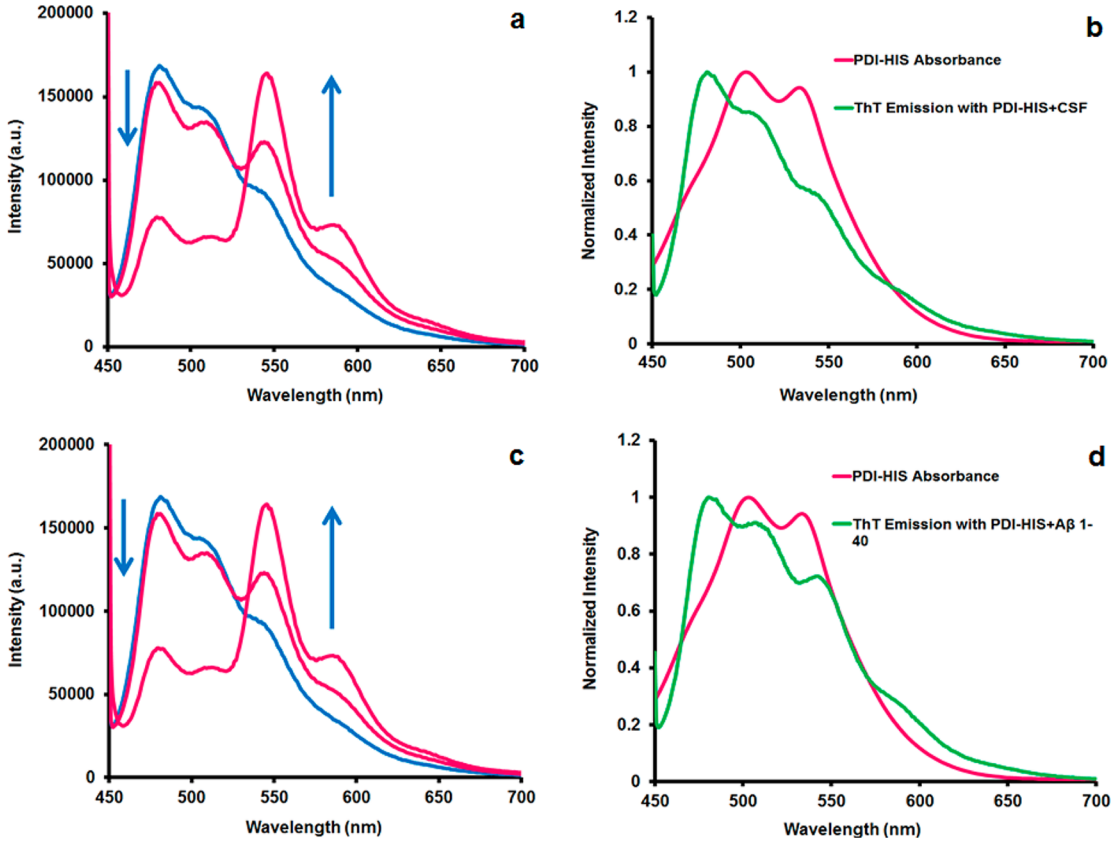

Figure 7. Monitoring Aβ1−40 aggregation by fluorescence resonance energy transfer (FRET) from ThT to PDI−HIS. (a and c) Emission spectra (excitation wavelength, 440 nm) of CSF and Aβ1−40 (0.76 μM) incubated at 37 °C from 0 to 72 h with PDI−HIS (0.33 μM) and ThT (20 μM). ThT emission λ_{max} = 488 nm. PDI−HIS emission λ_{max} = 546 nm. (b and d) Fluorescence resonance energy transfer (FRET) spectra obtained from donor ThT to PDI−HIS.

microrod structures are totally converted into mature microrod coassembled structures (Figure 6d,h) which are in agreement with the AFM and FE-SEM images. Finally, the obtained POM images confirm the modulation of Aβ1−40 and aggregates in CSF into coassembled mature microrod structure which are entirely different from the Aβ self-aggregates. For control studies, we performed similar experiments to confirm the formation of coassembled vesicles and mature rod-shaped structures in the absence of PDI−HIS with Aβ 1−40 fibrils (0.76 μM) and CSF Aβ fibrils (50 μL). The obtained images confirm that mature rod-shape structures were not observed in the absence of PDI−HIS with Aβ 1−40 fibrils and CSF Aβ fibrils even after 4 and 8 days incubation (Figure S4).

Modulating Effect of PDI−HIS Confirmed by FRET Study. The interaction of PDI−HIS with specific Aβ aggregates were examined by assessing the amount of Aβ aggregates from the fluorescence intensity of ThT fluorescence assay (0−72 h) (Figure 7). ThT does not bind with Aβ1−40 and Aβ1−42 monomers but ThT is a common fluorescent probe that could be used to quantify Aβ aggregates. Initially, the PDI−HIS (0.33 μM) was added into aggregated Aβ1−40 fibrils (0.76 μM) and CSF Aβ fibrils (50 μL) in the presence of ThT (20 μM) and kept for incubation (0−72 h) to monitor the fluorescence changes at 488 nm. The mixtures of both the solutions were excited at 440 nm and the emission peaks appeared at 488 nm predominantly at 0 h which confirms that no significant interaction has occurred between PDI−HIS and Aβ fibrils. After the samples were incubated (0−72 h), we screened ThT fluorescence changes at 488 nm for both the samples. Subsequently, we observed that PDI−HIS significantly quenched the fluorescence of ThT after interacting with Aβ fibrils and a new enhanced emission peak appeared at 546 nm at different time intervals (0−72 h) which strongly confirms that PDI−HIS modulates the Aβ fibrils.

To determine the mechanism of PDI−HIS binding and its influence on the Aβ1−40 aggregation, we monitored the Aβ1−40 aggregation over time in the presence of ThT with PDI−HIS. Increase in ThT fluorescence suggests that the compound may be inducing Aβ aggregation, while decrease in ThT fluorescence suggests that the compound modulates Aβ aggregation. Notably, the ThT emission band at 488 nm with PDI−HIS in the presence of Aβ1−40 fibril is much lower than in the absence of PDI−HIS, due to nonradiative energy transfer from ThT to PDI−HIS. On incubation of PDI−HIS in the presence of CSF Aβ fibrils and Aβ1−40 fibrils with ThT and excited them at 440 nm, we observed the ThT emission maximum at 488 nm with lower fluorescence intensity, but the significant emission band appeared at 546 nm (Figure 7a,c) due to the consistent energy transfer from the donor ThT into the acceptor PDI−HIS (FRET).[48] Consequently, the emission spectra of ThT with CSF aggregates and/or Aβ1−40 fibrils overlapped with the excitation spectra of PDI−HIS (Figure 7b,d), which confirms the mechanism of nonradiative transfer of ThT excited-state energy to PDI−HIS (FRET). Finally, this result strongly confirms that PDI−HIS could recognize and modulate the Aβ1−40 fibrils and aggregated fibrils in CSF by the noncovalent interaction induced coassembly mechanism.[49]

DOI: 10.1021/acsami.5b07260
ACS Appl. Mater. Interfaces 2015, 7, 21226−21234

CONCLUSIONS

In summary, we presented an extremely effective and complementary approach toward the modulation of amyloidogenic peptides by accelerating the aggregation process using a biocompatible fluorescent PDI−HIS molecule, which is different from inhibiting the aggregation of Aβ peptides. The formation of hybrid microrods in aqueous solution by the process of coassembly between Aβ1−40 fibrils and Aβ aggregates of CSF with PDI−HIS, was predominantly driven by noncovalent interactions. The modulating effect on Aβ1−40 and CSF aggregates were validated by ThT assay, FT-IR, fluorescence spectroscopy, DLS, AFM, FE-SEM, and POM which establishes that the histidine functionalized perylene diimide molecule accelerates the Aβ1−40 and the aggregates of CSF into micro size coassembled structures. Therefore, PDI−HIS molecular probe possesses a significant targeted modulating effect on Aβ1−40 fibrils and the Aβ fibrils of CSF by forming coassembled PDI−HIS+Aβ hybrids structure. Consequently, this could lead to potential design and development of drugs targeted toward AD.

ASSOCIATED CONTENT

Supporting Information

The Supporting Information is available free of charge on the ACS Publications website at DOI: 10.1021/acsami.5b07260.

Details of all the experiments and instrumentation. (PDF)

AUTHOR INFORMATION

Corresponding Author

*E-mail: pki@iitg.ernet.in.

Notes

The authors declare no competing financial interest.

ACKNOWLEDGMENTS

Financial support from the Department of Science and Technology (DST), India (No. DST/SERB/PC-20/2014/000034), (No. DST/TSG/PT/2009/11&23), DST−Max Planck Society, Germany (No. INT/FRG/MPG/FS/2008), Department of Information Technology, DeitY project No. 5(9)/2012−NANO (Vol. II). We thank Dr. C. Patra, IICT-Hyderabad, India, for performing the toxicity experiments.

REFERENCES

(1) Chiti, F.; Dobson, C. M. Protein Misfolding, Functional Amyloid, and Human Disease. *Annu. Rev. Biochem.* **2006**, *75*, 333−366.
(2) LaFerla, F. M.; Green, K. N.; Oddo, S. Intracellular Amyloid-Beta in Alzheimer's Disease. *Nat. Rev. Neurosci.* **2007**, *8*, 499−509.
(3) Roychaudhuri, R.; Yang, M.; Hoshi, M. M.; Teplow, D. B. Amyloid β-Protein Assembly and Alzheimer Disease. *J. Biol. Chem.* **2009**, *284*, 4749−4753.
(4) Hamley, I. W. The Amyloid Beta Peptide: A Chemist's Perspective. Role in Alzheimer's and Fibrillization. *Chem. Rev.* **2012**, *112*, 5147−5192.
(5) Takahashi, T.; Mihara, H. Peptide and Protein Mimetics Inhibiting Amyloid Beta-Peptide Aggregation. *Acc. Chem. Res.* **2008**, *41*, 1309−1318.
(6) Gordon, D. J.; Sciarretta, K. L.; Meredith, S. C. Inhibition of β-Amyloid(40) Fibrillogenesis and Disassembly of β-Amyloid(40) Fibrils by Short β-Amyloid Congeners Containing N-Methyl Amino Acids at Alternate Residues. *Biochemistry* **2001**, *40*, 8237−8245.
(7) Bard, F.; Cannon, C.; Barbour, R.; Burke, R.; Games, D.; Grajeda, H.; Guido, T.; Hu, K.; Huang, J.; Johnson-Wood, K.; Khan, K.; Kholodenko, D.; Lee, M.; Lieberburg, I.; Motter, R.; Nguyen, M.; Soriano, F.; Vasquez, N.; Weiss, K.; Welch, B.; Seubert, P.; Schenk, D.; Yednock, T. Peripherally Administered Antibodies against Amyloid Beta-Peptide Enter the Central Nervous System and Reduce Pathology in a Mouse Model of Alzheimer Disease. *Nat. Med.* **2000**, *6*, 916−919.
(8) McLaurin, J.; Cecal, R.; Kierstead, M. E.; Tian, X.; Phinney, A. L.; Manea, M.; French, J. E.; Lambermon, M. H. L.; Darabie, A. A.; Brown, M. E.; Janus, C.; Chishti, M. A.; Horne, P.; Westaway, D.; Fraser, P. E.; Mount, H. T. J.; Przybylski, M.; St George-Hyslop, P. Therapeutically Effective Antibodies against Amyloid-Beta Peptide Target Amyloid-Beta Residues 4−10 and Inhibit Cytotoxicity and Fibrillogenesis. *Nat. Med.* **2002**, *8*, 1263−1269.
(9) Crouch, P. J.; Barnham, K. J. Therapeutic Redistribution of Metal Ions to Treat Alzheimer's Disease. *Acc. Chem. Res.* **2012**, *45*, 1604−1611.
(10) Hindo, S. S.; Mancino, A. M.; Braymer, J. J.; Liu, Y.; Vivekanandan, S.; Ramamoorthy, A.; Lim, M. H. Small Molecule Modulators of Copper-Induced Aβ Aggregation. *J. Am. Chem. Soc.* **2009**, *131*, 16663−16665.
(11) Yang, F.; Lim, G. P.; Begum, A. N.; Ubeda, O. J.; Simmons, M. R.; Ambegaokar, S. S.; Chen, P. P.; Kayed, R.; Glabe, C. G.; Frautschy, S. A.; Cole, G. M. Curcumin Inhibits Formation of Amyloid Beta Oligomers and Fibrils, Binds Plaques, and Reduces Amyloid in vivo. *J. Biol. Chem.* **2005**, *280*, 5892−5901.
(12) Cavalli, A.; Bolognesi, M. L.; Capsoni, S.; Andrisano, V.; Bartolini, M.; Margotti, E.; Cattaneo, A.; Recanatini, M.; Melchiorre, C. A Small Molecule Targeting the Multifactorial Nature of Alzheimer's Disease. *Angew. Chem., Int. Ed.* **2007**, *46*, 3689−3692.
(13) Cabaleiro-Lago, C.; Quinlan-Pluck, F.; Lynch, I.; Lindman, S.; Minogue, A. M.; Thulin, E.; Walsh, D. M.; Dawson, K. A.; Linse, S. Inhibition of Amyloid β Protein Fibrillation by Polymeric Nanoparticles. *J. Am. Chem. Soc.* **2008**, *130*, 15437−15443.
(14) Yoo, S. I.; Yang, M.; Brender, J. R.; Subramanian, V.; Sun, K.; Joo, N. E.; Jeong, S.; Ramamoorthy, A.; Kotov, N. A. Inhibition of Amyloid Peptide Fibrillation by Inorganic Nanoparticles: Functional Similarities with Protein. *Angew. Chem., Int. Ed.* **2011**, *50*, 5110−5115.
(15) Geng, J.; Li, M.; Ren, J.; Wang, E.; Qu, X. Polyoxometalates as Inhibitors of the Aggregation of Amyloid β Peptides Associated with Alzheimer's Disease. *Angew. Chem., Int. Ed.* **2011**, *50*, 4184−4188.
(16) Le Droumaguet, B.; Nicolas, J.; Brambilla, D.; Mura, S.; Maksimenko, A.; De Kimpe, L.; Salvati, E.; Zona, C.; Airoldi, C.; Canovi, M.; Gobbi, M.; Magali, N.; La Ferla, B.; Nicotra, F.; Scheper, W.; Flores, O.; Masserini, M.; Andrieux, K.; Couvreur, P. Versatile and Efficient Targeting using a Single Nanoparticulate Platform: Application to Cancer and Alzheimer's Disease. *ACS Nano* **2012**, *6*, 5866−5879.
(17) Würthner, F.; Thalacker, C.; Sautter, A. Hierarchical Organization of Functional Perylene Chromophores to Mesoscopic Superstructures by Hydrogen Bonding and $\pi-\pi$ Interactions. *Adv. Mater.* **1999**, *11*, 754−758.
(18) Hirschberg, J. H. K. K.; Brunsveld, L.; Ramzi, A.; Vekemans, J. A. J. M.; Sijbesma, R. P.; Meijer, E. W. Helical Self-Assembled Polymers from Cooperative Stacking of Hydrogen-Bonding Pairs. *Nature* **2000**, *407*, 167−170.
(19) Yang, D. S.; Yip, C. M.; Huang, T. H. J.; Chakrabartty, A.; Fraser, P. E. Manipulating the Amyloid-Beta Aggregation Pathway with Chemical Chaperones. *J. Biol. Chem.* **1999**, *274*, 32970−32974.
(20) Urbanc, B.; Cruz, L.; Le, R.; Sanders, J.; Ashe, K. H.; Duff, K.; Stanley, H. E.; Irizarry, M. C.; Hyman, B. T. Neurotoxic Effects of Thioflavin S-Positive Amyloid Deposits in Transgenic Mice and Alzheimer's Disease. *Proc. Natl. Acad. Sci. U. S. A.* **2002**, *99*, 13990−13995.
(21) Alavez, S.; Vantipalli, M. C.; Zucker, D. J. S.; Klang, I. M.; Lithgow, G. J. Amyloid-Binding Compounds Maintain Protein Homeostasis During Ageing and Extend Lifespan. *Nature* **2011**, *472*, 226−229.
(22) Salomon, A. R.; Marcinowski, K. J.; Friedland, R. P.; Zagorski, M. G. Nicotine Inhibits Amyloid Formation by the Beta-Peptide. *Biochemistry* **1996**, *35*, 13568−13578.
(23) Claridge, S. A.; Thomas, J. C.; Silverman, M. A.; Schwartz, J. J.; Yang, Y.; Wang, C.; Weiss, P. S. Differentiating Amino Acid Residues and Side Chain Orientations in Peptides using Scanning Tunneling Microscopy. *J. Am. Chem. Soc.* **2013**, *135*, 18528−18535.

DOI: 10.1021/acsami.5b07260
ACS Appl. Mater. Interfaces 2015, 7, 21226−21234

(24) Kalashnyk, N.; Nielsen, J. T.; Nielsen, E. H.; Skrydstrup, T.; Otzen, D. E.; Laegsgaard, E.; Wang, C.; Besenbacher, F.; Nielsen, N. C.; Linderoth, T. R. Scanning Tunneling Microscopy Reveals Single-Molecule Insights into the Self-Assembly of Amyloid Fibrils. *ACS Nano* **2012**, *6*, 6882−6889.
(25) Mao, X.; Guo, Y.; Luo, Y.; Niu, L.; Liu, L.; Ma, X.; Wang, H.; Yang, Y.; Wei, G.; Wang, C. Sequence Effects on Peptide Assembly Characteristics Observed by using Scanning Tunneling Microscopy. *J. Am. Chem. Soc.* **2013**, *135*, 2181−2187.
(26) Ma, X. J.; Liu, L.; Mao, X. B.; Niu, L.; Deng, K.; Wu, W. H.; Li, Y. M.; Yang, Y. L.; Wang, C. Amyloid Beta (1−42) Folding Multiplicity and Single-Molecule Binding Behavior Studied with STM. *J. Mol. Biol.* **2009**, *388*, 894−901.
(27) Mao, X. B.; Wang, C. X.; Wu, X. K.; Ma, X. J.; Liu, L.; Zhang, L.; Niu, L.; Guo, Y. Y.; Li, D. H.; Yang, Y. L.; Wang, C. Beta Structure Motifs of Islet Amyloid Polypeptides Identified Through Surface-Mediated Assemblies. *Proc. Natl. Acad. Sci. U. S. A.* **2011**, *108*, 19605−19610.
(28) Liu, L.; Zhang, L.; Mao, X.; Niu, L.; Yang, Y.; Wang, C. Chaperon-Mediated Single Molecular Approach Toward Modulating Aβ Peptide Aggregation. *Nano Lett.* **2009**, *9*, 4066−4072.
(29) Liu, L.; Zhang, L.; Niu, L.; Xu, M.; Mao, X.; Yang, Y.; Wang, C. Observation of Reduced Cytotoxicity of Aggregated Amyloidogenic Peptides with Chaperone-like Molecules. *ACS Nano* **2011**, *5*, 6001−6007.
(30) Hard, T.; Lendel, C. Inhibition of Amyloid Formation. *J. Mol. Biol.* **2012**, *421*, 441−465.
(31) Necula, M.; Kayed, R.; Milton, S.; Glabe, C. G. Small Molecule Inhibitors of Aggregation Indicate that Amyloid β Oligomerization and Fibrillization Pathways are Independent and Distinct. *J. Biol. Chem.* **2007**, *282*, 10311−10324.
(32) Bucciantini, M.; Giannoni, E.; Chiti, F.; Baroni, F.; Formigli, L.; Zurdo, J. S.; Taddei, N.; Ramponi, G.; Dobson, C. M.; Stefani, M. Inherent Toxicity of Aggregates Implies a Common Mechanism for Protein Misfolding Diseases. *Nature* **2002**, *416*, 507−511.
(33) Muthuraj, B.; Chowdhury, S. R.; Mukherjee, S.; Patra, C. R.; Iyer, P. K. Aggregation Deaggregation Influenced Selective and Sensitive Detection of Cu^{2+} and ATP by Histidine Functionalized Water-soluble Fluorescent Perylene Diimide under Physiological Conditions and in Living Cells. *RSC Adv.* **2015**, *5*, 28211−28218.
(34) Chen, S.; Wetzel, R. Solubilization and Disaggregation of Polyglutamine Peptides. *Protein Sci.* **2001**, *10*, 887−891.
(35) Hortschansky, P.; Schroeckh, V.; Christopeit, T.; Zandomeneghi, G.; Fändrich, M. The Aggregation Kinetics of Alzheimer's β-Amyloid Peptide is Controlled by Stochastic Nucleation. *Protein Sci.* **2005**, *14*, 1753−1759.
(36) Muthuraj, B.; Hussain, S.; Iyer, P. K. A Rapid and Sensitive Detection of Ferritin at a Nanomolar Level and Disruption of Amyloid β Fibrils using Fluorescent Conjugated Polymer. *Polym. Chem.* **2013**, *4*, 5096−5107.
(37) Hindo, S. S.; Mancino, A. M.; Braymer, J. J.; Liu, Y.; Vivekanandan, S.; Ramamoorthy, A.; Lim, M. H. Small Molecule Modulators of Copper-Induced Aβ Aggregation. *J. Am. Chem. Soc.* **2009**, *131*, 16663−16665.
(38) Ma, Q.; Wei, G.; Yang, X. Influence of Au Nanoparticles on the Aggregation of Amyloid-β-(25−35) Peptides. *Nanoscale* **2013**, *5*, 10397−10403.
(39) Ban, T.; Hamada, D.; Hasegawa, K.; Naiki, H.; Goto, Y. Direct Observation of Amyloid Fibril Growth Monitored by Thioflavin T Fluorescence. *J. Biol. Chem.* **2003**, *278*, 16462−16465.
(40) D'Amico, M.; Schiro, G.; Cupane, A.; D'Alfonso, L.; Leone, M.; Militello, V.; Vetri, V. High Fluorescence of Thioflavin T Confined in Mesoporous Silica Xerogels. *Langmuir* **2013**, *29*, 10238−10246.
(41) Dwivedi, A. K.; Iyer, P. K. Therapeutic Strategies to Prevent Alzheimer's Disease Pathogenesis Using A Fluorescent Conjugated Polyelectrolyte. *Macromol. Biosci.* **2014**, *14*, 508−514.
(42) Chen, B.; Thurber, K. R.; Shewmaker, F.; Wickner, R. B.; Tycko, R. Measurement of Amyloid Fibril Mass-Per-Length by Tilted-Beam Transmission Electron Microscopy. *Proc. Natl. Acad. Sci. U. S. A.* **2009**, *106*, 14339−14344.
(43) Campioni, S.; Carret, G.; Jordens, S.; Nicoud, L.; Mezzenga, R.; Riek, R. The Presence of an Air−Water Interface Affects Formation and Elongation of α-Synuclein Fibrils. *J. Am. Chem. Soc.* **2014**, *136*, 2866−2875.
(44) Jansen, R.; Dzwolak, W.; Winter, R. Amyloidogenic Self-Assembly of Insulin Aggregates Probed by High Resolution Atomic Force Microscopy. *Biophys. J.* **2005**, *88*, 1344−1353.
(45) Ridgley, D. M.; Ebanks, K. C.; Barone, J. R. Peptide Mixtures can Self-assemble into Large Amyloid fibers of Varying Size and Morphology. *Biomacromolecules* **2011**, *12*, 3770−3779.
(46) Dehn, S.; Castelletto, V.; Hamley, I. W.; Perrier, S. Altering Peptide Fibrillization by Polymer Conjugation. *Biomacromolecules* **2012**, *13*, 2739−2747.
(47) Nilsson, M. R.; Dobson, C. M. In vitro Characterization of Lactoferrin Aggregation and Amyloid Formation. *Biochemistry* **2003**, *42*, 375−382.
(48) Lee, J.; Culyba, E. K.; Powers, E. T.; Kelly, J. W. Amyloid-β forms Fibrils by Nucleated Conformational Conversion of Oligomers. *Nat. Chem. Biol.* **2011**, *7*, 602−609.
(49) Tagliavini, F.; Forloni, G.; Colombo, L.; Rossi, G.; Girola, L.; Canciani, B.; Angeretti, N.; Giampaolo, L.; Peressini, E.; Awan, T.; De Gioia, L.; Ragg, E.; Bugiani, O.; Salmona, M. Tetracycline Affects Abnormal Properties of Synthetic Prp Peptides and PrP(Sc) in vitro. *J. Mol. Biol.* **2000**, *300*, 1309−1322.

DOI: 10.1021/acsami.5b07260
ACS Appl. Mater. Interfaces 2015, 7, 21226−21234